

# White Dendrimer Organic Light Emitting Diodes: Exciton Formation and Transfer

Lorenz Graf von Reventlow, Wei Jiang, Dani M. Stoltzfus, Steven M. Russell, Paul L. Burn,\* and Alexander Colsmann\*

In this work solution-processed organic white-light emitting diodes comprising a blend of red and blue phosphorescent dendrimers are presented. In contrast to common small molecule blended-dye organic light emitting diodes (OLEDs), the bulky dendrons between the light emitting moieties increase the spacing and hamper the transfer of excitons between the dyes. The reduced transfer of the excitons from the blue dye to the red dye enables greater control over OLED color avoiding the issue in which small variations in the concentration of the red dye can dramatically change the emission color. Thus, the approach leads to enhanced manufacturing reproducibility. Transient electroluminescence measurements provide detailed insights into the charge carrier and exciton formation and transfer dynamics within the device.

## 1. Introduction

For the generation of white light in organic light emitting diodes (OLEDs) different device architectures have been reported, including the implementation of two or more monochromatic devices into tandem-OLEDs,<sup>[1,2]</sup> the stacking of multiple emission layers (EML) in a single OLED<sup>[3]</sup> or the blending of emitter molecules (dyes) with complementary emission spectra within one layer.<sup>[4–7]</sup> All device concepts have been implemented in vacuum-deposited and solution-processed OLEDs. Tandem OLEDs


are the mainstream industrial implementation of white OLEDs since they benefit from a reduced current density, which can lead to an enhancement in operational lifetime.<sup>[8]</sup> However, tandem devices are difficult to fabricate using solution methods as the sequential deposition of the many functional layers requires orthogonal solvents or solvent barriers.<sup>[2]</sup> Instead, blending all the dyes into one emission layer enhances the manufacturability, requiring fewer layers and hence reducing costs and manufacturing time. Typically, white OLEDs comprise a narrow-energy-gap dye (typically red-orange emission) and a wide-energy-gap dye (typically blue emission), but also more than two dyes can be implemented for

better spectral coverage. Such blended-dye OLEDs exhibit complex charge carrier and exciton dynamics where excitons can be generated on the host ( $g_h$ ), on the blue dye ( $g_b$ ), or on the red dye ( $g_r$ ), and excitons can transfer from the host to either dye ( $k_{hb}$  and  $k_{hr}$ ) or from the blue dye to the red dye ( $k_{br}$ ) by energy transfer.<sup>[8]</sup> **Figure 1** illustrates these exciton generation and transfer pathways. Given the concentrations of the dyes in the film, the overlap of the emission and absorption spectra (Figure S2, Supporting Information) and the relatively low extinction coefficients, energy transfer from the blue to the red dye is most likely to occur via Dexter energy transfer (DET). The emission color is then determined by the ratio of radiative exciton decay on the blue dye and the red dye, the latter of which depends on the concentration of the red dye, the relative energy levels of the blue and red dyes, and the DET rate ( $k_{br}$ ) from the blue to the red dye. Although this concept is commonly employed to generate white light from phosphorescent or thermally activated delayed fluorescence (TADF) dyes, it has one important disadvantage. Due to the often very efficient DET, the concentration of the red dyes has to be more than one order of magnitude smaller than the concentration of the blue dye in order to generate similar amounts of photons, i.e., typically on the order of 0.1 wt% for the red dye and 10 wt% for the blue dye.<sup>[4–7]</sup> Small variations in the dye concentrations can therefore lead to strong shifts in color,<sup>[9]</sup> which requires precise control of the dye concentrations, hampering the manufacturability and hence the industrial uptake of this concept. Using blue dendrimer TADF dyes doped with small molecular phosphorescent emitters<sup>[10]</sup> or blue TADF dyes with strong steric hinderance doped with yellow TADF emitters<sup>[11]</sup> enabled larger amounts of narrow-energy-gap dyes (5 and 2 wt%, respectively), hence enhancing the controllability of the OLED color.

L. Graf von Reventlow, Dr. A. Colsmann  
Karlsruhe Institute of Technology (KIT)  
Light Technology Institute  
Engesserstrasse 13, Karlsruhe 76131, Germany  
E-mail: alexander.colsmann@kit.edu

L. Graf von Reventlow, Dr. A. Colsmann  
Karlsruhe Institute of Technology (KIT)  
Material Research Center for Energy Systems  
Strasse am Forum 7, Karlsruhe 76131, Germany

Dr. W. Jiang, Dr. D. M. Stoltzfus, Dr. S. M. Russell, Prof. P. L. Burn  
Centre for Organic Photonics & Electronics  
The School of Chemistry and Molecular Biosciences  
The University of Queensland  
Queensland 4072, Australia  
E-mail: P.burn2@uq.edu.au

 The ORCID identification number(s) for the author(s) of this article can be found under <https://doi.org/10.1002/adom.202001289>.

© 2020 The Authors. Published by Wiley-VCH GmbH. This is an open access article under the terms of the Creative Commons Attribution License, which permits use, distribution and reproduction in any medium, provided the original work is properly cited.

DOI: 10.1002/adom.202001289

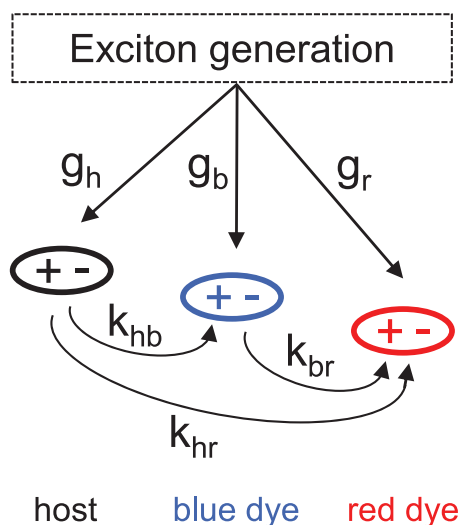


**Figure 1.** Illustration of the generic exciton generation and transfer pathways in a blended-dye white OLED.

In this work, we reduce the color variability of blended-dye white OLEDs and improve the process reproducibility against variations of the dye concentration by diminishing the DET from the blue to the red dye using molecular engineering. In order to increase the spacing between the dyes, we implement dendronized dyes, in which the dendrons shield the light emitting core.<sup>[12]</sup> We investigate how the DET rate is affected by molecular spacing and how and where, under these circumstances, excitons are formed. All the investigations were carried out on operational OLEDs and hence in the most relevant environment.

## 2. White OLEDs Comprising Blends of Dendronized Dyes

To investigate the effect of dye spacing and reduction of exciton transfer, we fabricated blended-dye OLEDs comprising either dendronized dyes or, for reference, literature-known nondendronized dyes, and varied the dye blend ratio. The experiments were carried out using the first generation dendrimer emitters **D-blue** and **D-red**, which are depicted in **Figure 2a**. The luminescent cores of the dyes are marked with the respective emission color. The dendrons attached to the ligands of the phosphorescent iridium(III) complex enhance the solubility and exhibit higher exciton energies, with the latter point leading to the emission occurring from iridium(III) complex at the core. The dendrimers were soluble in a range of polar aprotic solvents (e.g., dichloromethane, chloroform, tetrahydrofuran, and toluene), with the choice of solvent used for the fabrication of the devices governed by the solubility of the host material. The synthesis of **D-blue** is described in the Supporting Information, the synthesis of **D-red** was reported in our earlier work.<sup>[13]</sup> The blue and red dyes, bis[2-(4,6-difluorophenyl)pyridinato-C<sup>2</sup>,N](picolinato)iridium(III) (FIrpic) and bis(2-methyldibenzo[*f,h*]quinoxaline)(acetylacetonate)iridium(III) (Ir(MDQ)<sub>2</sub>(acac)), which have comparable photoluminescence quantum yields (PLQYs)

and phosphorescence lifetimes were used as nondendronized references. Throughout the experiments, we varied the ratio between red and blue dyes while maintaining the overall dye concentration of 5 wt%. All OLEDs were fabricated according to the layer sequence depicted in **Figure 2b**, comprising indium tin oxide (ITO)/poly(3,4-ethylenedioxythiophene):polystyrene sulfonate (PEDOT:PSS)/3,3'-di(9*H*-carbazol-9-yl)biphenyl (mCBP) doped with 5 wt% dye/3,3',5,5'-tetra[*m*-pyridyl]-phen-3-yl]biphenyl (BP4mPy)/8-hydroxyquinolato-lithium (Liq)/aluminum (Al). The PEDOT:PSS hole transport layer (HTL) and the emission layer were spin-coated from solution. In order to enhance the reproducibility of the device fabrication and hence the comparability of the devices, the BP4mPy electron transport layer (ETL) as well as the Liq/Al top electrode were deliberately deposited by vacuum sublimation. The energy levels of the materials are shown in **Figure 2b**, with the ionization potentials (IPs) of **D-blue** and **D-red** measured using photoelectron spectroscopy in air. The smaller IP of **D-blue** when compared to **D-red** is consistent with the oxidation potentials measured using cyclic voltammetry, which were 0.2 and 0.4 V<sup>[13]</sup> (against the ferrocene/ferrocenium couple), respectively (**Figure S1**, Supporting Information). While the reductions of **D-red** could be measured using cyclic voltammetry, those for **D-blue** could not be observed within the solvent window. These results indicated that electron injection into **D-blue** would be expected to be more difficult than for **D-red**, with the reverse for holes. The IPs and electron affinities (EAs) of mCBP<sup>[14]</sup> and BP4mPy<sup>[15]</sup> were taken from the literature.

Notably, the OLEDs and hence the dyes **D-red** and **D-blue** exhibited good stability throughout the experiments, even during multiple current density–voltage (*J*–*V*) sweeps, which was reflected in a stable external quantum efficiency (EQE). We did observe some increase of the driving voltage during multiple *J*–*V* sweeps, which is known issue with mCBP arising from degradation in the presence of excited states—see Supporting Information for details.<sup>[14]</sup> A full summary of device data, i.e., luminous efficacies, current efficiencies and color rendering indices (CRIs) is provided (**Table S1** and **Figure S3**, Supporting Information).

In our reference OLEDs comprising nondendronized dyes with a blue-to-red dye ratio of 3:2 w/w we observed almost no emission from FIrpic but strong emission from Ir(MDQ)<sub>2</sub>(acac) (**Figure 2c**). This is very much in accordance with other reports on white OLEDs with blended (nondendronized) dyes, where efficient DET results in the need for much higher concentrations of the blue dye to achieve white emission.<sup>[16]</sup> At the same blue-to-red dye w/w ratio, the dendrimer-OLED comprising **D-blue** and **D-red** still emitted a substantial amount of blue light, indicating a reduced transfer of excited states from **D-blue** to **D-red** by DET, which in part is due to the higher molar ratio of the blue emitter in comparison to the nondendronized dyes. Even at a **D-blue**:**D-red** blend ratio of 2.5:2.5 w/w, a molar ratio similar to the nondendronized dyes with a blue-to-red dye ratio of 3:2 w/w, a significant contribution to the emission spectrum from **D-blue** is visible. As depicted in the emission spectra in **Figure 2d** and the color coordinates of the OLEDs in the inset of **Figure 2e**, the emission color can be linearly tuned from sky-blue to red by varying the blend ratio of **D-blue** and **D-red**. This reduced sensitivity of the OLED color on small changes of the

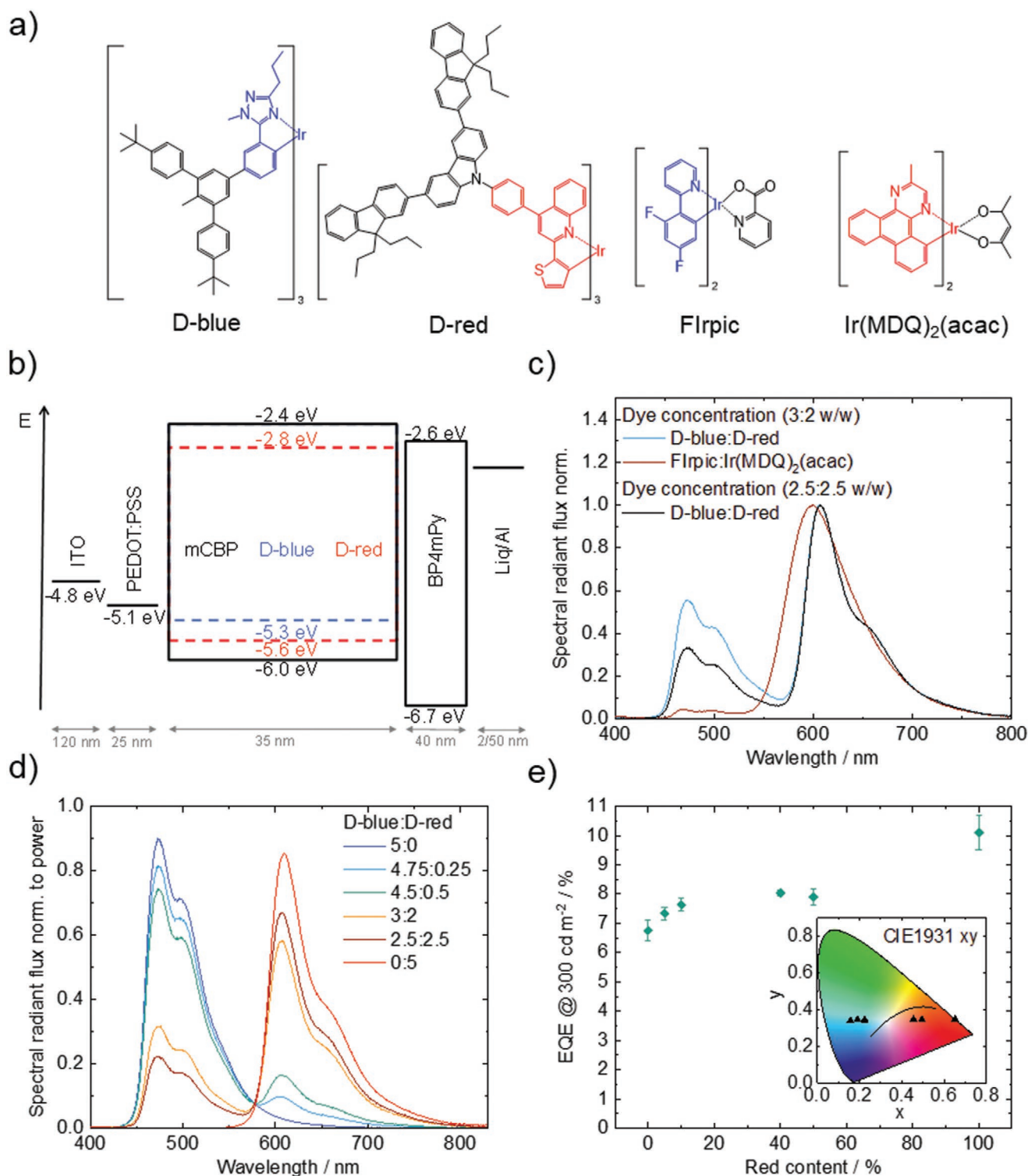


**Figure 2.** a) Structures of the dyes. The emissive “core” is marked with the respective color. Both dendrimers are first generation, with the blue comprising biphenyl dendrons with t-butyl surface groups and the red having bis(fluorenyl)carbazole dendrons with n-propyl surface groups. b) Energy level diagram of the OLED stack. The layer thicknesses measured by white-light interferometry are indicated beneath the layers. c) Electroluminescence spectrum of the dendrimer OLED with a dye concentration of 3:2 w/w (**D-blue:D-red**) and the reference device with the same weight ratio. The dendrimer OLED with a ratio of 2.5:2.5 w/w has the same molar ratio as the reference device (62:38 mol/mol). d) Emission spectra of the dendrimer OLEDs with different dye ratios. e) EQE of the dendrimer OLEDs at 300 cd m<sup>-2</sup> comprising **D-blue** and **D-red** at different ratios. Inset: CIE1931-diagram of the dendrimer OLEDs.

dye concentration marks a significant advance over state-of-the-art blended-dye OLEDs.

### 3. Energy Transfer from D-Blue to D-Red

In Section 2 we observed that the color of the OLEDs is less sensitive to the concentration of the dendronized dyes than in the reference OLED comprising nondendronized dyes. That is, there is always a significant blue component, even at a weight ratio of 2.5:2.5 w/w. In all cases, the ratio of the integrated blue and red component of the emission is smaller than the molar ratios of the two materials, which implies either that more excitons are generated on **D-red** than on **D-blue**, or that, despite protection of the emissive cores by the dendrons, some excitons transfer from **D-blue** to **D-red**. To unravel the exciton dynamics behind this balanced color, we investigated the DET from **D-blue** to **D-red**.

A first estimation of the amount of energy that is transferred from **D-blue** to **D-red** can be gained from fitting the emission spectra. The fit is based on the assumption that the exciton generation mechanisms are similar in the blended-dye and monochromatic devices and that the EQE only depends on the PLQY of the dyes. The parameters of the fit are the molar dye ratios, the EQE of the corresponding monochromatic devices (Supporting Information) and the transfer of excitons from **D-blue** to **D-red** in percent (%). As the molar dye ratios and the EQEs are known, the only unknown parameter is the energy transfer. The best fit was achieved for a transfer of 44% of the excitons on **D-blue** to **D-red**. The EQE of the dendrimer OLEDs increased with the content of **D-red** from EQE = 7% for a neat blue device to EQE = 10% for a neat red device at  $300 \text{ cd m}^{-2}$ , which we attribute to the higher photoluminescence quantum yield of **D-red** versus **D-blue** (78% vs 47% in mCBP, Figure 2e). The fact that the EQEs were slightly lower than the theoretical maximum based on PLQYs and standard outcoupling from the device is most probably due to electron leakage from the emission layer into the PEDOT:PSS (as discussed below).

Second, we tracked the exciton transfer rate,  $k_{br}$ , between **D-blue** and **D-red** (Figure 1) by transient electroluminescence (EL) of OLEDs with different dye blend ratios. Transient EL can be used to monitor exciton generation and transfer as well as charge carrier trapping in the actual device configuration.<sup>[17,18]</sup> We performed transient EL on the monochromatic and blended-dendrimer OLEDs by applying a voltage pulse with an amplitude  $A = +8 \text{ V}$ . A small pulse width of  $\Delta t = 500 \text{ ns}$  ensured negligible heat load on the OLED and hence mitigated device degradation during the measurements. The voltage pulses were repeated with a frequency of 1 kHz. The histogram of the photon emission delays produced transients that represent the electroluminescence decay. The spectrally separated emission of the dyes allowed the differentiation of both their electroluminescence transients. **D-blue** exhibits a characteristic emission at 480 nm, whereas **D-red** shows an emission peak at 620 nm, with minimal overlap between the two emission spectra. As depicted in Figure 3a, the exciton lifetime of the blue dendrimer **D-blue** is reduced upon intermixing of the red dendrimer **D-red**, and it continues to decrease if the concentration of **D-red** is increased. Likewise, we observed a delayed emission

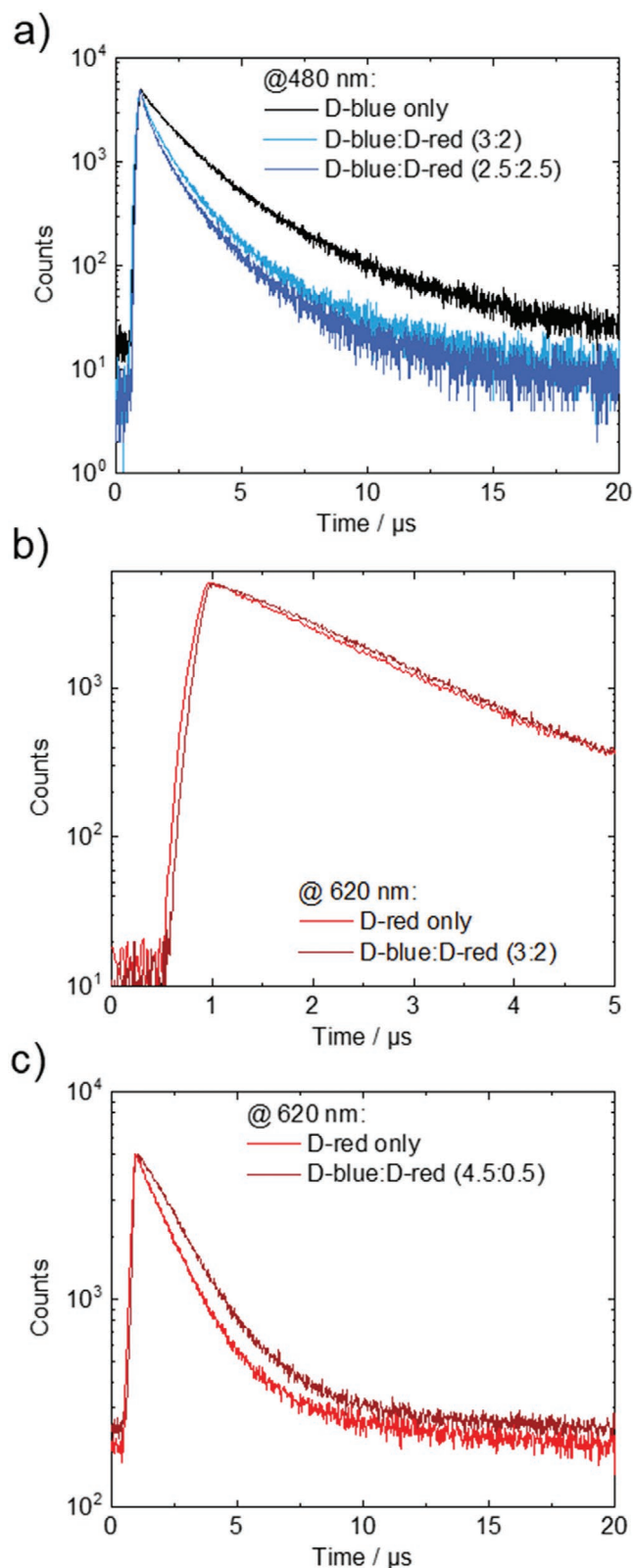


**Figure 3.** a) Transient EL decay of the blue emission (repetition rate: 1 kHz) and b) transient EL decay of the red emission (repetition rate: 1 kHz). c) The delayed red emission becomes even more apparent at a **D-blue:D-red** blend ratio of 4.5:0.5 w/w (repetition rate: 50 kHz).



of **D-red** if **D-blue** is intermixed (Figure 3b). The smaller change of the red transient for a ratio of 3:2 w/w compared to the blue transient indicates that excitons are not only transferred from **D-blue** to **D-red** ( $k_{br}$ ) but are also generated directly on **D-red** ( $g_r$ ). As a result, the delay is more pronounced for lower **D-red** concentrations where direct exciton generation on **D-red** is less likely (Figure 3c). Together, these observations are strong indications for DET from **D-blue** to **D-red** ( $k_{br}$ ). Assuming that the position of the emission zone prevails for different **D-blue**:**D-red** ratios at an overall constant dye concentration, we conclude a constant Purcell-factor and therefore equal radiative decay rates of the blue excitons in all OLEDs. Based on these assumptions, the only process that reduces the exciton lifetime of **D-blue** is exciton transfer to **D-red**. Therefore, by integration of the blue EL-transients we can calculate the relative number of excitons on **D-blue** that are quenched by **D-red**. For a weight ratio of 3:2 w/w (7:3 molar ratio) of **D-blue**:**D-red**, 42% of the blue excitons are transferred to **D-red**. This is in very close agreement with our previous estimation of 44%, which we derived from the spectrum fitting process above, indicating that about half of the excitons on **D-red** were transferred from **D-blue** by DET. The other half is either directly generated on **D-red** from trapped electrons and holes or transferred from the host. Likewise, at a ratio of 2.5:2.5 w/w, the amount of transferred excitons from **D-blue** to **D-red** increases to 52%, also calculated from the integrals of the electroluminescence transient, which also nicely matches the data derived from the spectral fit above. This increase in DET is a logical consequence of the decreased average distance between **D-blue** to **D-red** macromolecules when the **D-red** concentration is increased. Importantly, the two independent methods and analyses yielded similar results. Transient EL measurements of FIrpic:Ir(MDQ)<sub>2</sub>(acac) OLEDs show stronger quenching of the blue emission (Supporting Information), in accordance with the emission spectrum in Figure 2c. Altogether, in contrast to state-of-the-art blended-dye OLEDs, the strongly reduced DET between the blue and the red dye leads to greater control over the spectral shape and solves the issue of where a small change in dye ratio can lead to a very large change in emission color.

#### 4. Bias-Dependent Color Shift

Not only does the dye concentration affect the emission color of the white OLEDs. As depicted in Figure 4a, we also observed an enhanced blue emission at higher operation voltages and hence higher luminance. In the literature, such voltage-dependent color shifts are attributed to the trapping of charge carriers.<sup>[19–21]</sup> A color shift due to saturation of red dye sites, as it is sometimes reported, is unlikely as the density of dye molecules typically exceeds the charge carrier density by several orders of magnitude.<sup>[19]</sup> A saturation would only occur for very low dye concentrations, which does not apply here. Yet, charge carrier trapping can change the color of the white OLED: at higher operating voltages and internal electrical fields, the relative number of charge carriers trapped on **D-red** and **D-blue** may change due to differences in the bias-dependency of the charge carrier trapping rate versus the unperturbed charge carrier transport through the emissive layer.<sup>[19,20]</sup>

Trapped charge carriers can remain in the device for several milliseconds.<sup>[22]</sup> Radiative recombination of the trapped charge carriers can produce a continuous but very weak luminescence on the ms timescale. Again, transient EL measurements allow the monitoring of this longer-lived population of charge carriers. We pumped the reservoir of trapped charge carriers at different rates by changing the repetition rate of the voltage pulse. The duration  $\Delta t = 500$  ns and amplitude  $A = 8$  V of the pulses and hence the photon flux per pulse were kept the same. Figure 4b,c depict the electroluminescence transients at voltage pulse rates of 1, 10, and 50 kHz in the blue (480 nm) and in the red (620 nm). The magnitude of the transients on the right side (towards 20  $\mu$ s) are indicative of the population of trapped charge carriers in the device. Hence, we interpret the increasing magnitude of the transients for higher repetition rates as an increased population of trapped charge carriers. The magnitude of the transients before the pulse on the left side indicates that the charge carriers may remain in the device for several hundred microseconds, i.e., at least until the next voltage pulse is applied. The turn-on time of the electroluminescence transient also provides information on the lifetime of the charge carriers in the OLED.<sup>[22]</sup> According to the transient in the red regime (Figure 4c), the OLED starts to emit earlier at higher repetition rates due to the trapped charge carriers from the previous voltage pulse that do not have to travel through the transport layers. This is a second indication that charge carriers that lead to red emission are stored in the device for at least 1 ms, which is the time between two voltage pulses. Interestingly, the blue transients (Figure 4b) exhibit similar turn-on times at repetition rates of 10 and 1 kHz. This lets us conclude that the charge carriers that lead to blue emission, have a lifetime of less than 100  $\mu$ s.

Since both **D-blue** and **D-red** are triplet emitters with an exciton lifetime below 5  $\mu$ s, we exclude long lasting phosphorescence or triplet-triplet-annihilation as the origin of the delayed electroluminescence. Storage of triplet excitons on the host and subsequent delayed transfer to the dyes also appears unlikely, since the **D-red** has larger dendrons than **D-blue**, which results in on average a larger distance between the host molecules and the light emitting core of **D-red** compared to **D-blue**. Such a simple analysis would lead to the expectation of better exciton transfer from the host to **D-blue** (than to **D-red**) and hence a stronger transient magnitude in the blue, which is opposite to our observations. However, it is important to remember that these singly dendronized materials have the dendrons attached to a facial iridium(III) complex core, which means that the dendrimers have a cone shape with one face of the emissive core more open to contact with the host and/or adjacent emissive materials.

Individual charge carriers in OLEDs can populate trap states or build space charges at interfaces. While positive space charges (holes) may well accumulate at the interface with the BP4mPy hole blocking layer, it is unlikely that negative space charges (electrons) would build up at the interface to the PEDOT:PSS layer due to its conductivity. Thus, if electrons remain within the device, they would be expected to preferentially populate trap states. In contrast to excitons, individual charge carriers respond to an electrical field. To get further evidence that such individual charge carriers in the OLED

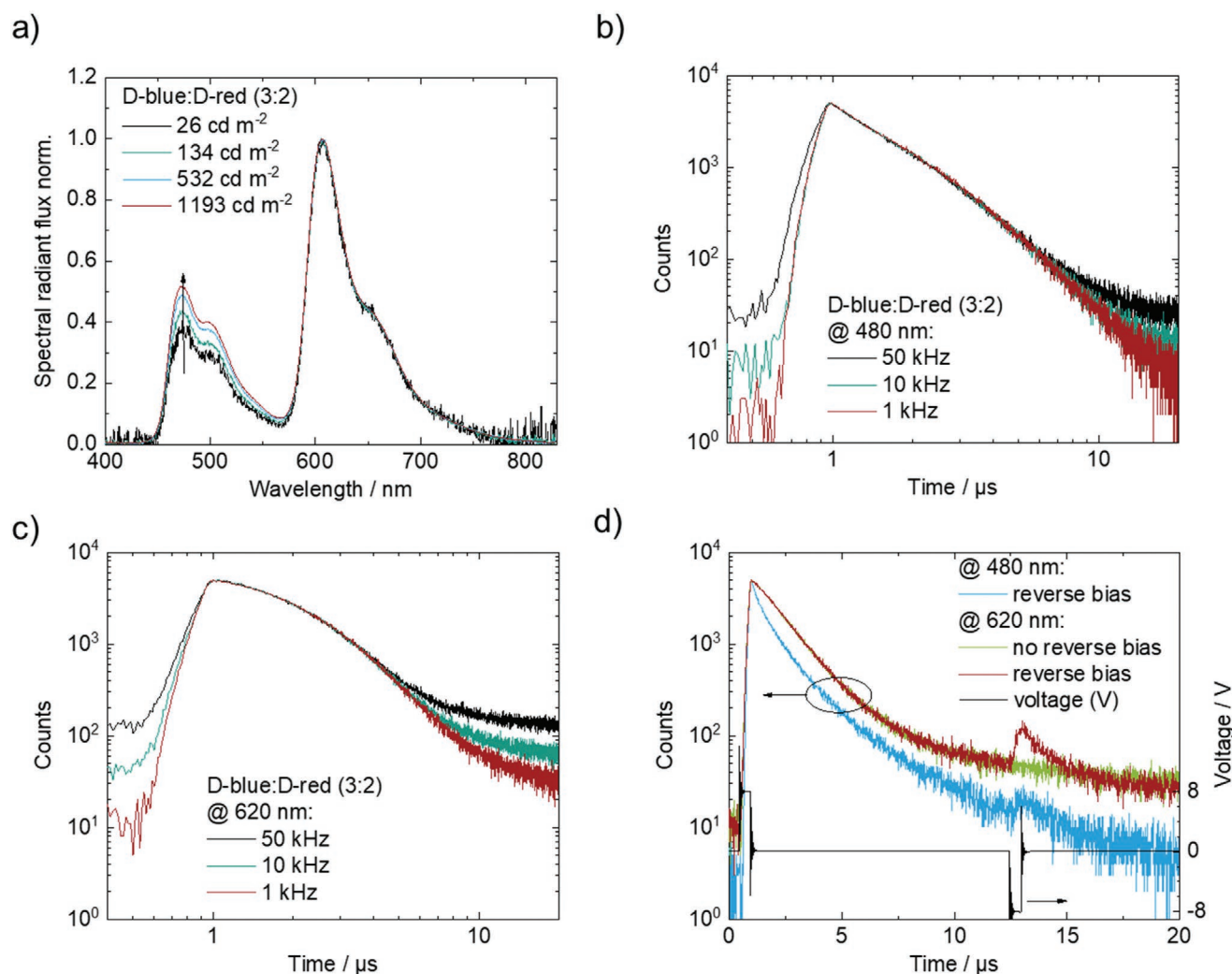


**Figure 4.** a) Bias-dependent color shift of a white dendrimer OLED. Transient EL of b) **D-blue** and c) **D-red** at different voltage pulse repetition rates in a double-logarithmic plot. d) Transient EL of the red emission with and without an intermediate reverse bias pulse (repetition rate: 1 kHz). The measured voltage over the OLED (with reverse bias pulse) is displayed on the right vertical axis. The same reverse bias pulse has almost no effect on the blue emission. The RC time-constant of the OLED is much smaller than the phosphorescence lifetime of the dyes.

remain after the voltage pulse is switched off, we applied a negative voltage pulse after 12  $\mu\text{s}$  with the same amplitude and duration as the forward pulse (Figure 4d, black line, right axis). Figure 4d compares the transients of the OLED at 620 nm with and without this reverse pulse. The reverse pulse induced a strong overshoot in the transient emission of **D-red**, immediately upon application of the voltage pulse. Its decay has a monoexponential time constant of 1.2  $\mu\text{s}$  which we attribute to the phosphorescence lifetime of **D-red**. This positive overshoot indicates that electrons and holes drift towards each other during the reverse pulse.<sup>[18]</sup> Altogether, these measurements and the energetics of the OLED layer stack (Figure 2b) indicate that electrons do not accumulate at either interface of the emissive layer but must be trapped within the emission layer itself. Based on the reduction potentials/EAs of the materials, it would be expected that **D-red** acts as an electron trap, which is why the delayed emission from **D-red** is stronger than the delayed emission from **D-blue**. On

the other side, holes accumulate at the BP4mPy interface, from where they can drift towards the HTL under reverse bias to recombine with the trapped electrons ( $g_r$ ). At 480 nm (**D-blue**, Figure 4d), we observed a much weaker and hardly visible overshoot which leads us to conclude that **D-blue** plays only a minor role in the storage of charge carriers in the device that lead to photon emission. To investigate if excitons are generated on mCBP ( $g_h$ ) and transferred to **D-blue** ( $k_{hb}$ ) or **D-red** ( $k_{hr}$ ), we examined the EL-spectrum of the OLEDs. We observed weak emission below 400 nm in the electroluminescence spectra, which we attribute to mCBP emission, and hence conclude that some excitons are also generated on the host (Figure S4, Supporting Information). From the excitation of the host and the corresponding photoluminescence spectra (Supporting Information), we infer that the singlet exciton transfer from mCBP to both dyes is quite efficient. To what extent triplet excitons transfer between the host and the dyes and if excitons are generated on **D-blue** ( $g_b$ ) remains open.

We note that the OLED color dependence on the operation voltage plays only a minor role in the operation of white OLEDs as their brightness is commonly controlled by pulse-width modulation.

## 5. White OLEDs with Improved Color Rendering

To unravel the energy transfer processes, we have deliberately blended two complementary emitting dyes which, depending on their ratio, produced colors along a line between sky-blue and red color coordinate in the CIE1931 diagram. For lighting applications however, not only a white color but also a good spectral coverage is important for improved color rendering. To enhance the green/yellow emission of the blended-dye dendrimer OLEDs we added a third, yellow-emitting dendrimer into the blend. The resulting OLED showed similar performance with an EQE of 8% (Figure 5a,b). Adding the yellow-green emitting dendrimer **D-yellow**<sup>[23]</sup> into the blend resulted

in a broad emission spectrum (Figure 5c). The result is a warm-white OLED with color coordinates  $(x;y) = (0.45;0.40)$  and an improved CRI = 78 (vs a maximal CRI = 45 for **D-blue:D-red** emission). These coordinates are located right on the Planckian locus with a correlated color temperature of 2830 K, matching the color temperature of halogen lamps.

## 6. Conclusions

This work is the first comprehensive investigation of exciton dynamics in blended phosphorescent dendrimer-dyes for white light generation in OLEDs. The dendrimeric encapsulation of the dyes provides spacing between the light emitting moieties for reduced exciton transfer from the blue to the red dye. As a consequence, the color of the OLED is much less affected by small variations of the dye concentration as it is often observed in state-of-the-art small molecule blended-dye OLEDs, facilitating reproducible device fabrication and

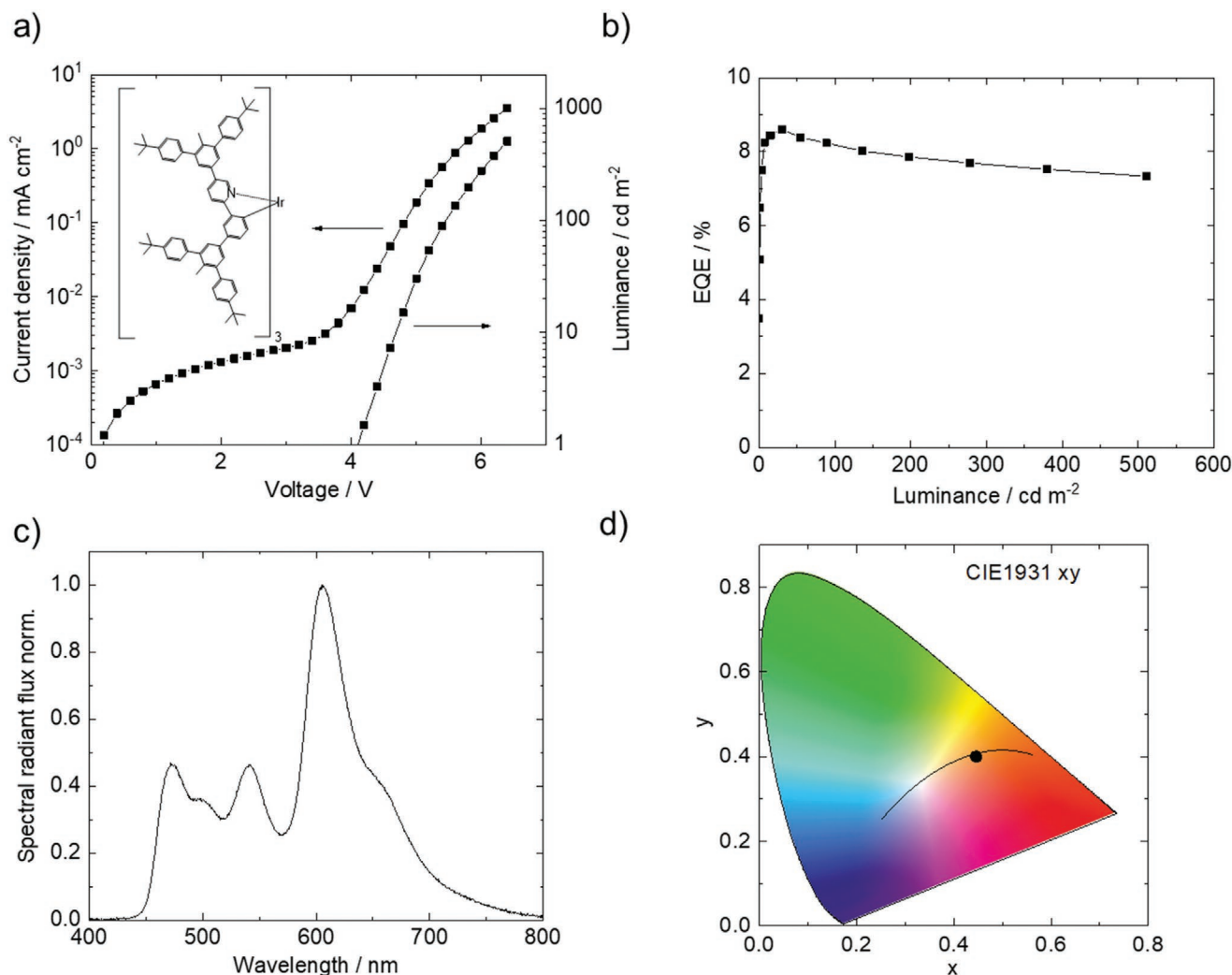


**Figure 5.** a)  $J$ - $V$ - $L$  characteristics of a white dendrimer OLED comprising **D-blue** (3 wt%), **D-yellow** (0.25 wt%), and **D-red** (1.75 wt%). Inset: structure of **D-yellow**. b) External quantum efficiency. c) Emission spectrum of the **D-blue:D-yellow:D-red** OLED at 510 cd m<sup>-2</sup>. d) CIE1931  $xy$  diagram with the color coordinates of the warm-white OLED.

color control. Detailed transient electroluminescence studies revealed not only a reduced DET from the blue to the red dye, but also a direct transfer of the charge carriers on the mCBP host to the red dendrimer dye. The combination of device characteristics and the charge carrier dynamics demonstrates the superiority of the dendrimer-dye-concept for blended-dye emission layers. Blending a third, yellow-emitting dendrimer dye into the blend resulted in a warm-white OLED with a good color rendering index of 78 and a correlated color temperature of 2830 K.

## 7. Experimental Section

**OLED Fabrication:** Prestructured ITO substrates were sequentially sonicated in acetone and 2-propanol for 10 min each, before they were treated with oxygen plasma for 2 min. Immediately after plasma cleaning they were transferred to a nitrogen-filled glovebox where a layer of PEDOT:PSS (VPAI 4083 from Heraeus; diluted 1:3 v/v in ethanol) was spincoated (4000 rpm, 45 s) and annealed at 120 °C for 10 min. For the emission layer, mCBP, **D-blue** and **D-red** were dissolved in tetrahydrofuran (THF) at a total solid concentration of 3 g L<sup>-1</sup>. The total concentration of **D-blue** and **D-red** in mCBP was 5 wt%. The weight ratio of **D-blue** and **D-red** was varied. The emission layer was spin-coated (3000 rpm, 45 s) and then annealed at 80 °C for 10 min to remove any residual solvents. Afterwards the substrates were transferred to a customized multichamber thermal evaporator (base pressure 1E-7 mbar) where the electron transport layer (BP4mPy, 40 nm, 1 Å s<sup>-1</sup>), the electron injection layer (Liq, 2 nm, 0.1 Å s<sup>-1</sup>), and the aluminum electrode (50 nm, 0.5–2 Å s<sup>-1</sup>) were thermally evaporated without breaking vacuum. The active area of 10.5 mm<sup>2</sup> was defined by the overlap of the electrodes. mCBP, Liq and BP4mPy were purchased from Lumtec.

**Characterization:** The *J*–*V* characteristics of the OLEDs were recorded with a Keithley 2400 source measurement unit. The luminous flux was measured in a glovebox in a high reflectance integrating sphere (19 cm diameter, Gigahertz Optik) coupled to a spectrometer (CASI40CT-151, Instrument Systems) and a photometer (VL-1101-2, Gigahertz Optik). The luminance was calculated from the luminous flux, assuming Lambertian emission. The edges of the substrates were covered, ensuring only forward facing surface emission to enter the sphere. The sphere was calibrated using a halogen lamp luminance standard with 2 $\pi$ -emission and with known spectrum and luminous flux. The calibration of the lamp is traceable to the Physikalisch Technische Bundesanstalt (PTB). A halogen aiding lamp accounted for the different absorption of the OLEDs and the calibration lamp. The photometer response (we consider the combination of sphere and detector as photometer, not only the photodiode) was corrected by a spectral mismatch correction factor to account for the difference of the spectra of the calibration lamp and the OLEDs as well as the change of the photometer response caused by different absorption of the OLEDs and the calibration lamp. Three measurements were needed to calculate the luminous flux of the OLEDs: (1) The raw spectrum and raw luminous flux of the aiding lamp with the calibration lamp in the sphere. (2) The raw spectrum and raw luminous flux of the aiding lamp with the OLED (device under test) in the sphere. (3) The raw spectrum and raw luminous flux of the OLED. The luminous flux was then calculated according to the formula in the Supporting Information. The OLEDs were not driven until their maximum achievable luminance to prevent degradation and hence to ensure comparability of all the measurements that were carried out on the same device.

**Transient Electroluminescence Measurement:** Transient electroluminescence was measured in an Edinburgh Instruments FS5 fluorometer with the multichannel scaling technique. The OLEDs were driven by a voltage pulse generator (Keysight 81150A, amplitude *A* = 8 V, pulse duration  $\Delta t$  = 500 ns) with an internal resistance of 5  $\Omega$ , and the voltage over the OLED was measured with an oscilloscope (Keysight DSO-S 104A). During the measurements, the sample chamber was flushed with nitrogen to prevent

quenching of triplet states by oxygen. After the transient measurements, the efficiency of the OLEDs was measured again in an integrating sphere to verify no device degradation during the pulsed measurements.

## Supporting Information

Supporting Information is available from the Wiley Online Library or from the author.

## Acknowledgements

L.G.v.R. and A.C. acknowledge support by the Helmholtz program “Science and Technology of Nanosystems” (STN). P.L.B. acknowledges the Helmholtz International Fellow Award under which the exchange of scientists and this collaborative work was made possible. The synthesis of the materials was supported by an Australian Research Council Laureate Fellowship awarded to P.L.B. (FL160100067). The fluorometer was made available under grant no. 03EK3571 (project TAURUS2), funded by the German Ministry for Education and Research (BMBF).

Open access funding enabled and organized by Projekt DEAL.

## Conflict of Interest

The authors declare no conflict of interest.

## Keywords

dendrimers, exciton dynamics, organic light emitting diodes, transient electroluminescence, white-light generation

Received: July 30, 2020  
Revised: September 23, 2020  
Published online:

- [1] F. Guo, D. Ma, *Appl. Phys. Lett.* **2005**, *87*, 1.
- [2] S. Höfle, A. Schienle, C. Bernhard, M. Bruns, U. Lemmer, A. Colsmann, *Adv. Mater.* **2014**, *26*, 5155.
- [3] S. Reineke, F. Lindner, G. Schwartz, N. Seidler, K. Walzer, B. Lüssem, K. Leo, *Nature* **2009**, *459*, 234.
- [4] R. Wang, D. i Liu, R. Zhang, L. Deng, J. Li, *J. Mater. Chem.* **2012**, *22*, 1411.
- [5] S. F. Wu, S. H. Li, Y. K. Wang, C. C. Huang, Q. Sun, J. J. Liang, L. S. Liao, M. K. Fung, *Adv. Funct. Mater.* **2017**, *27*, 1.
- [6] B. Zhang, G. Tan, C. S. Lam, B. Yao, C. L. Ho, L. Liu, Z. Xie, W. Y. Wong, J. Ding, L. Wang, *Adv. Mater.* **2012**, *24*, 1873.
- [7] D. Zhang, L. Duan, Y. Zhang, M. Cai, D. Zhang, Y. Qiu, *Light: Sci. Appl.* **2015**, *4*, 1.
- [8] Y. Yin, M. U. Ali, W. Xie, H. Yang, H. Meng, *Mater. Chem. Front.* **2019**, *3*, 970.
- [9] Z. Wu, D. Ma, *Mater. Sci. Eng., R* **2016**, *107*, 1.
- [10] X. Liao, X. Yang, R. Zhang, J. Cheng, J. Li, S. Chen, J. Zhu, L. Li, *J. Mater. Chem. C* **2017**, *5*, 10001.
- [11] D. Ding, Z. Wang, C. Li, J. Zhang, C. Duan, Y. Wei, H. Xu, *Adv. Mater.* **2020**, *1906950*, 1.
- [12] a) S.-C. Lo, N. A. H. Male, J. P. J. Markham, S. W. Magennis, P. L. Burn, O. V. Salata, I. D. W. Samuel, *Adv. Mater.* **2002**, *14*, 975; b) S.-C. Lo, T. D. Anthopoulos, E. B. Namdas, P. L. Burn, I. D. W. Samuel, *Adv. Mater.* **2005**, *17*, 1945.
- [13] S. M. Russell, A. M. Brewer, D. M. Stoltzfus, J. Saghaei, P. L. Burn, *J. Mater. Chem. C* **2019**, *7*, 4681.



- [14] A. S. D. Sandanayaka, T. Matsushima, C. Adachi, *J. Phys. Chem. C* **2015**, *119*, 23845.
- [15] S.-J. Su, D. Tanaka, Y.-J. Li, H. Sasabe, T. Takeda, J. Kido, *Org. Lett.* **2008**, *10*, 941.
- [16] a) L. Hou, L. Duan, J. Qiao, D. Zhang, G. Dong, L. Wang, Y. Qiu, *Org. Electron.* **2010**, *11*, 1344; b) B. W. D'Andrade, R. J. Holmes, S. R. Forrest, *Adv. Mater.* **2004**, *16*, 624.
- [17] a) P. Wang, S. Zhao, Z. Xu, B. Qiao, Z. Long, Q. Huang, *Molecules* **2016**, *21*, 1365; b) M. Regnat, K. P. Pernstich, S. Züfle, B. Ruhstaller, *ACS Appl. Mater. Interfaces* **2018**, *10*, 31552; c) R. Liu, Z. Gan, R. Shinar, J. Shinar, *Phys. Rev. B* **2011**, *83*, 1; d) H. Zamani Siboni, Y. Luo, H. Aziz, *J. Appl. Phys.* **2011**, *109*, 044501.
- [18] C. Weichsel, L. Burtone, S. Reineke, S. I. Hintschich, M. C. Gather, K. Leo, B. Lüssem, *Phys. Rev. B* **2012**, *86*, 075204.
- [19] Q. Wang, J. Ding, D. Ma, Y. Cheng, L. Wang, X. Jing, F. Wang, *Adv. Funct. Mater.* **2009**, *19*, 84.
- [20] M. C. Gather, R. Alle, H. Becker, K. Meerholz, *Adv. Mater.* **2007**, *19*, 4460.
- [21] H. T. Nicolai, A. Hof, P. W. M. Blom, *Adv. Funct. Mater.* **2012**, *22*, 2040.
- [22] J.-H. Lee, S. Lee, S.-J. Yoo, K.-H. Kim, J.-J. Kim, *Adv. Funct. Mater.* **2014**, *24*, 4681.
- [23] D. M. Stoltzfus, W. Jiang, A. M. Brewer, P. L. Burn, *J. Mater. Chem. C* **2018**, *6*, 10315.